Kinetic effects on the toroidal ion pressure gradient drift mode

KINETIC EFFECTS ON THE TOROIDAL ION PRESSURE GRADIENT DRIFT MODE

P. TERRY, W. ANDERSON, W. HORTON
Institute for Fusion Studies,
University of Texas at Austin,
Austin, Texas,
United States of America

ABSTRACT. The question of the threshold of the ion pressure gradient drift mode in toroidal geometry is examined from the drift-kinetic equation retaining the grad-B and curvature drift resonances of the ions with the mode. Analytic criteria for the onset of the instability are derived which exhibit the parametric dependence on toroidicity, pressure gradient and perpendicular wavenumber.

1. INTRODUCTION

Recently, there has been renewed in interest in drift modes in toroidal geometry in order to more fully understand both the linear stability and the non-linear evolution. From fluid theory, Horton et al. [1] have analysed the ballooning toroidal drift mode driven by the ion pressure gradient, an instability previously considered by Coppi and Pegoraro [2]. In Ref. [1], the surface eigenvalue problem from the ballooning-mode theory of drift waves [3] is solved for the parametric dependence of the eigenmode frequency ω_k and growth rate γ_k on the dimensionless parameters $(\epsilon_n, \eta_i, \xi, q, k)$ and compared with the analytic formulas obtained from the strong-ballooning limit. The dimensionless parameters are (i) the toroidicity $\epsilon_n = r_n/R$, (ii) the ion temperature-to-density gradient parameter η_i, (iii) the shear $\xi = rq'/q$, (iv) the inverse rotational transform $q = rB_0/RB_\theta$, and (v) the perpendicular azimuthal wavenumber measured with respect to the ion gyroradius $k = k_\theta \rho$ with $\rho = c(m_i T_e)^{1/2}/eB$. In this study, all frequencies are measured in units of c_s/r_n, where the ion-acoustic speed is $c_s = (T_e/m_i)^{1/2}$, and we consider $T_e = T_i$, for simplicity.

The eigenmode study of Horton et al. [1] shows that there are two regimes for instability. For weak toroidicity and strong shear, $\xi > 2q$, the mode occurs as in the sheared slab model of Coppi et al. [4] with a growth rate proportional to the square root of the shear parameter. The non-linear saturation and the anomalous thermal transport of this regime are reported in the three-dimensional fluid simulations of Horton et al. [5]. The second regime, $\xi < 2q$, corresponds to typical tokamak parameters. Here, the mode balloons significantly to the outside of the torus and can be described as the ion pressure gradient drift mode driven by the locally unfavourable magnetic curvature. In the simplest limit, the growth rate is proportional to the parameter $\gamma_0 = [2\epsilon_n(1+\eta_i)]^{1/2}$. Since the magnetic curvature is favourable on the inside of the torus, the instability of the mode depends on the extent to which the mode balloons to the outside. Analysis of the surface eigenvalue problem [6] shows that the condition $kq \gtrless \epsilon_n^{1/2}$ differentiates the mode structures which are, respectively, strongly ballooning and hence fluid-unstable, and weakly ballooning and fluid-stable. For plasma pressure, $\beta = 8\pi p/B^2$, below the magnetohydrodynamic pressure limit $\beta < \epsilon_n/q^2$, the oscillations remain electrostatic in polarization.

2. TOROIDAL DRIFT MODE DISPERSION RELATIONS

The azimuthal phase velocity of the pressure-gradient-driven toroidal mode is small compared to the ion diamagnetic drift velocity, and thus the resonances of the ion grad-B and curvature drift can exert an important influence on the stability of the mode. The influence of the drift resonance is not considered in the works of Coppi and Pegoraro [2] and Horton et al. [1]. We note that, for general parameters, there are two kinetic resonances $\omega_k = k_\parallel v_\parallel$ and $\omega_k = \omega_{Di}$ that must be considered. Using the formulas for the eigenmode parameters ω_k, γ_k and $\bar{k}_\parallel$ given in Eqs (5), (7), and (12) of Ref.[1], it is found that the breakdown of the fluid expansion occurs from the $\omega_k = k_\parallel v_\parallel$ resonance in the slab regime ($\xi > 2q$) and from the

drift resonance in the toroidal regime ($\xi<2q$). Here, we restrict consideration to the toroidal regime where, for $kq>\epsilon_n^{1/2}$ and $\xi<2q$, the mode is ballooning and the dispersion relation is approximately independent of both ξ and q as is shown by Fig.3 of Ref.[1]. In what follows, we shall study the effects of the drift resonance on the stability of the toroidal system as a function of (ϵ_n, η_i, k).

The drift-kinetic equation for low-frequency electrostatic waves determines the fluctuating part of the ion distribution function through

$$f_{ik}(v_\perp, v_\parallel) = -\frac{e_i\phi_k}{T_i} F_M + h_k(v_\perp, v_\parallel) \exp[i(\vec{k}\times\vec{v}\cdot\hat{b})/\Omega_i] \qquad (1)$$

where the non-adiabatic part of the distribution satisfies

$$(\omega - v_\parallel \hat{k}_\parallel - \omega_D) h_k(v_\perp, v_\parallel) = [\omega - \omega_{*i}(E)] F_M(E) J_0\left(\frac{k_\perp v_\perp}{\Omega_i}\right)\left(\frac{e\phi_k}{T_i}\right) \qquad (2)$$

with

$$\omega_{*i}(E) = \frac{k_\theta c T_i}{e_i B n_i}\frac{dn_i}{dr}\left[1+\eta_i\left(E-\frac{3}{2}\right)\right]$$

$$\omega_D(v_\perp, v_\parallel) = -\frac{k_\theta c m_i}{e_i BR}\left(\frac{1}{2}v_\perp^2 + v_\parallel^2\right)(\cos\theta + \xi\theta\sin\theta)$$

and $\hat{k}_\parallel = -i(qR)^{-1}\partial/\partial\theta$. The background ion distribution is taken as Maxwellian $F_M(E)$ with the local temperature gradient $\eta_i = \partial_r \ln T_i(r)/\partial_r \ln n_i(r)$ and $J_0(k_\perp v_\perp/\Omega_i)$ is the finite-gyroradius Bessel function. The electrons are taken as adiabatic, $n_{ek} = n_e(e\phi_k/T_e)$, and the dispersion relation is obtained from quasi-neutrality.

We now analyse the condition under which the $v_\parallel\hat{k}_\parallel$-contribution to the ion resonance is weak compared with the ω_D-contribution. In the ballooning-mode study in Ref.[1], Section 3, the parametric dependence of the average $\bar{k}_\parallel$ in the normal mode is given. From this, it follows that the condition $\gamma_k > \bar{k}_\parallel c_s$ leads to the condition $1+\eta_i > \epsilon_n(\xi/q)^2$ (using Eq.(12) of Ref.[1]). For the toroidal regime $\xi<q$, the condition for neglecting the $k_\parallel v_\parallel$ resonance is less restrictive than the requirement for neglecting the ω_D-resonance, namely $|\omega_k + i\gamma_k| > 2k\epsilon_n$. Here, we restrict attention to the regime $\omega \sim \omega_D > \bar{k}_\parallel c_s$ in determining the effects of the drift resonances on the stability of the ballooning mode. Within this regime the toroidal dispersion relation is given by

$$\frac{T_i}{T_e} + 1 - \int d\underset{\sim}{v}\, F_M(E)\, J_0^2\left(\frac{k_\perp v_\perp}{\Omega}\right) \times \left[\frac{\omega-\omega_{*i}(E)}{\omega-\omega_D(v_\perp, v_\parallel)}\right] = 0 \qquad (3)$$

In the following, we restrict the study to $T_i = T_e$ and use the dimensionless wavenumber $k\theta c_s/\Omega_i = k$ and frequencies $\omega r_n/c_s = \omega$. Letting $t = m_i v_\perp^2/2T$ and $u = v_\parallel/(2T/m_i)^{1/2}$ the full kinetic dispersion relation in dimensionless variables becomes

$$\epsilon_k^{2d}(\omega) = 2-\pi^{-\frac{1}{2}}\int_0^\infty dt \int_{-\infty}^{+\infty} du \times \exp(-t-u^2) J_0^2(k\sqrt{2t}) \times \left[\frac{\omega + k(1-\frac{3}{2}\eta_i) + k\eta_i(t+u^2)}{\omega + k\epsilon_n(t+2u^2)}\right] = 0 \qquad (4)$$

The full kinetic dispersion relation (4) has been evaluated numerically and is discussed further in the Appendix.

2.1. The grad-B model

For modes with azimuthal phase velocities ω/k greater than the drift velocity ϵ_n, the grad-B resonance at $v_\perp^2 = \text{const}$ selects a larger region of velocity space than the curvature resonances at $v_\parallel^2 = \text{const}$. Thus we are motivated to introduce a non-resonant approximation to the u integral in relation (4). We call this approximation the grad-B model and replace Eq.(4) by

$$\epsilon_k(\omega) = 2 - \int_0^\infty dt \frac{\exp(-t)\left[\omega + k\left(1+\eta_i(t-1)\right)\right] J_0^2(k\sqrt{2t})}{\omega + 2k\epsilon_n t} = 0 \qquad (5)$$

The grad-B model has the same fluid limit as the full kinetic dispersion relation. The virtue of the grad-B

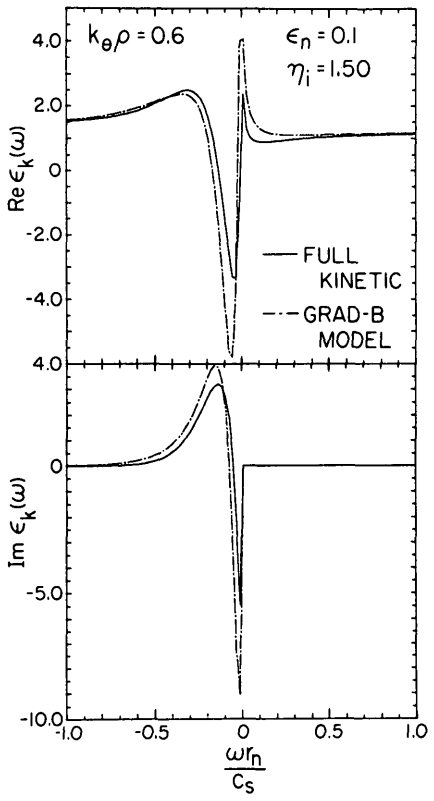

FIG. 1. The real and imaginary parts of the dispersion relation as a function of ω compared between the grad-B model $\epsilon_k(\omega)$ [Eq.(5)] and the full kinetic dispersion function $\epsilon_k^{2d}(\omega)$[Eq.(4)].

model dispersion relation is that it permits analytic stability criteria to be derived. In Fig.1, we show the differences between the exact and grad-B model dispersion relations by plotting $\epsilon_k(\omega)$ and $\epsilon_k^{2d}(\omega)$ for typical system parameters. From this figure, we note that the approximation produces a shift in the values of ω but otherwise reproduces the important features of the function. We have found that the shift does not affect the conclusions we draw from the Nyquist diagrams. As discussed further in the Appendix, however, the numerical differences become appreciable for large values of $\epsilon_n (\epsilon_n \lesssim 0.25)$.

2.2. The small-wavenumber limit

In Eqs (4) and (5), we take $k>0$ and have for $\omega \gtrless 0$ modes rotating in the electron or ion diamagnetic directions, respectively. We perform the integration on the fluid part of the integrand by writing $(\omega-\omega_D)^{-1} = \omega^{-1} + \omega_D[\omega(\omega-\omega_D)]^{-1}$, an exact transformation. In this section, we restrict our attention to small values of k^2 so that we can make the approximation $J_0^2 \cong 1-k^2t$. In Section 2.3, we give results for large k. Kinetic effects associated with the finite argument of the Bessel function have been analysed by Coppi and Pegoraro [2], but in the non-resonant limit only.

Defining $D(\omega) = \omega\epsilon(\omega)$ and dropping terms of higher order in $k^2\epsilon_n$, the simplified dispersion relation becomes

$$D_k(\omega) = \omega - ku_k + 2\epsilon_n k^2 \times \int_0^\infty \frac{dt[1+\eta_i(t-1)]t\exp(-t)}{\omega + 2\epsilon_n kt} \qquad (6)$$

where the phase velocity of the electron drift wave is $u_k = [1-2\epsilon_n - k^2(1+\eta_i)]/(1+k^2)$. For $k<k_0 = [(1-2\epsilon_n)/(1+\eta_i)]^{1/2}$, the drift wave rotates in the electron diamagnetic direction.

It is convenient to define explicitly the fluid dispersion relation $D(\omega)$ used in previous studies that follows from the kinetic dispersion relation (6) when $|\omega| > 2\epsilon_n k$. The fluid dispersion relation is

$$D(\omega) = \omega - ku_k + k^2 2\epsilon_n(1+\eta_i)/\omega \qquad (7)$$

with the unstable wavenumber band given by

$$u_k^2 < 4\gamma_0^2$$

or

$$k_0\left(1-\frac{2\gamma_0}{1-2\epsilon_n}\right)^{\frac{1}{2}} \lesssim k \lesssim k_0\left(1+\frac{2\gamma_0}{1-2\epsilon_n}\right)^{\frac{1}{2}} \qquad (8)$$

where $\gamma_0 = (2\epsilon_n)^{1/2}(1+\eta)^{1/2}$. The maximum growth rate occurs for $k \cong k_0$ and has $\gamma_m = (2\epsilon_n)^{1/2}$ which occurs in the fluid domain when $|1+\eta_i| > 2\epsilon_n$ as already noted.

We analyse the stability of the kinetic dispersion relation in terms of the Nyquist diagram method. For the Nyquist diagram, the imaginary part of $D(\omega)$ is plotted against the real part of $D(\omega)$ as ω ranges from $-\infty$ to $+\infty$. For large $|\omega|$, the integral part of $D(\omega)$ vanishes and $D(\omega) \cong D_f(\omega) \cong \omega$ so that the semi-circle in the upper half plane maps into the same semi-circle in the D-plane. The number of unstable roots of $D(\omega) = 0$ is then given by the number of times the map of $D(\omega)$ for real ω encloses the origin. Since a range of values of k is considered it is more useful to make

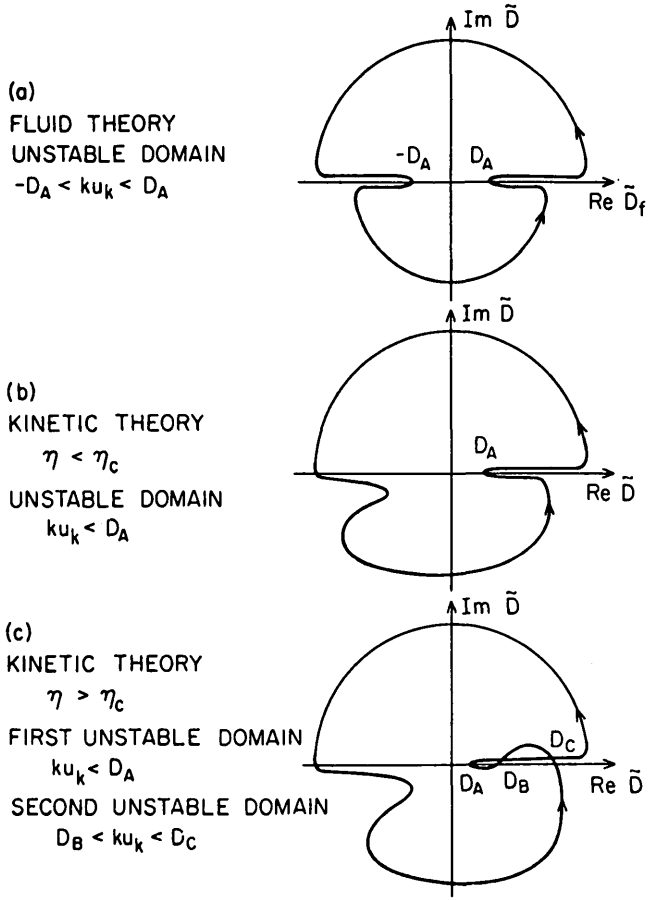

FIG.2. The Nyquist map of the dispersion relation $\tilde{D}(\omega)$ shown in (a) for the fluid theory in Eq.(15); (b) for the kinetic theory below the critical gradient, Eq.(16); and (c) for the kinetic theory above the critical gradient, Eqs (17) and (18).

the map of $\tilde{D}_k(\omega) = D_k(\omega) + ku_k$ and choose ku_k such that the origin is encircled when the topology of the $\tilde{D}_k(\omega)$ map permits such an origin-encircling choice of ku_k. The three $\tilde{D}$-maps derived here are shown in Fig.2.

For real, negative ω, the perturbation rotates in the ion diamagnetic direction and resonates with the local ion drift frequency to give

$$\mathrm{Im}D_k(\omega) = \pi k\left[1-\eta_i\left(\frac{\omega}{2\epsilon_n k}+1\right)\right] \times \left(\frac{\omega}{2\epsilon_n k}\right) \exp\left(\frac{\omega}{2\epsilon_n k}\right) \tag{9}$$

For $\eta_i > 1$, this function has two roots, one at $\omega = 0$ and one at $\omega_1 = -2\epsilon_n k(1-1/\eta_i)$. Im $\tilde{D}_k$ is positive for $\omega_1 < \omega < 0$ and negative for $\omega < \omega_1$. As $\omega \to -\infty$, $\mathrm{Im}\tilde{D}_k(\omega)$ approaches zero from the negative side. On the other hand, for $0 \leqslant \eta_i \leqslant 1$, the only root occurs at $\omega = 0$. Here, $\mathrm{Im}\tilde{D}_k(\omega)$ is negative-definite, growing quadratically for ω near zero, then decaying exponentially to zero as $\omega \to -\infty$. Thus, there is a critical value of the temperature gradient η_c above which the Nyquist diagram changes character. In the grad-B model, the value of the critical gradient is given by $\eta_c = 1$.

For positive values of ω where the perturbation rotates in the electron diamagnetic direction there are no resonances. For ω infinitesimally above the real ω axis, the sign of Im $\tilde{D}_k(\omega)$ changes at the minimum of the Re $\tilde{D}_k(\omega)$ since $\mathrm{Im}\tilde{D}_k(\omega) = i\delta[\partial\tilde{D}_k(\omega)/\partial\omega]$ where $\omega = \lim(\omega + i\delta)$ as $\delta \to 0^+$. Thus, the second critical frequency for the Nyquist diagram is given by

$$1 - 2\epsilon_n k^2 \int_0^\infty \frac{dt[1+\eta_i(t-1)]t\exp(-t)}{(\omega_2+2\epsilon_n kt)^2} = 0 \tag{10}$$

We now need the real parts of $\tilde{D}_k(\omega)$ evaluated at ω_1 and ω_2. Evaluation of $\tilde{D}_k(\omega)$ at $\omega = \omega_1$ is straightforward and gives

$$\tilde{D}_k(\omega_1) = k[\eta_i - 2\epsilon_n(1-1/\eta_i)] \quad \text{for} \quad \eta_i > 1 \tag{11}$$

We also easily obtain that $\tilde{D}_k(0) = k$. To determine $\tilde{D}_k(\omega_2)$, we find it convenient to evaluate $\tilde{D}_k(\omega)$ in terms of the exponential integral $E_1(x)$ [7] using $z = \omega/2k\epsilon_n$ to obtain

$$\tilde{D}_k(\omega = 2\epsilon_n kz) = k\left\{2\epsilon_n z + 1 - \eta_i z + ze^z E_1(z)[\eta_i(z+1)-1]\right\} \tag{12}$$

with the minimum of $\tilde{D}_k(\omega)$ determined by the roots of

$$1 + 2\epsilon_n - \eta_i(2+z) + e^z E_1(z) \times [\eta_i z^2 + z(3\eta_i - 1) + \eta_i - 1] = 0 \tag{13}$$

With a transcendental function specifying the root ω_2, it is useful to consider two limits. One limit

corresponds to small ϵ_n or large z for which an asymptotic expansion of $E_1(\omega/2\epsilon_n k)$ in powers of $\epsilon_n^{1/2}$ is possible. This is effectively the regime of validity of fluid theory. We shall find that the kinetic results, while altering the Nyquist topology give stability criteria which are compatible with those of a fluid theory computed to a sufficiently high order in the parameter $\epsilon_n^{1/2}$. The other limit is $\epsilon_n \geq 1$ or z small. In this limit, it is necessary to evaluate $E_1(z)$ numerically.

For small ϵ_n, we carry out the asymptotic expansion of $E_1(z)$ and find that, to second order, the root ω_2 is given by

$$\omega_2 = k[(2\epsilon_n)(1+\eta_i)]^{\frac{1}{2}} - \frac{4k\epsilon_n(1+2\eta_i)}{1+\eta_i} + O(\epsilon_n^{3/2})$$

and that the value of the dispersion function at ω_2 is given by

$$\mathrm{Re}\tilde{D}_k(\omega_2) = 2k[(2\epsilon_n)(1+\eta_i)]^{\frac{1}{2}} - 4k\epsilon_n \frac{(1+2\eta_i)}{1+\eta_i} \qquad (14)$$

From this information, it is straightforward to construct the Nyquist diagram of the dispersion relation as shown in Fig.2.

For the purpose of discussion, the critical points on the Nyquist curve are labelled A, B, and C, corresponding to the critical frequencies $\omega = \omega_2$, $\omega = 0$, and $\omega = \omega_1$, respectively. In Fig.2a, we show the Nyquist diagram for the fluid dispersion relation valid for $|\omega| > 2k\epsilon_n$. This diagram is symmetric in $\omega \to -\omega^*$. In the fluid regime, the condition that the map of $\tilde{D}(\omega)$ encircle the origin gives the instability condition

$$-\tilde{D}_A < ku_k < \tilde{D}_A \qquad (15)$$

where $\tilde{D}_A = \tilde{D}(\omega_A) = 2k\gamma_0$. Condition (15) reproduces the unstable wavenumber band given in Eq.(8) and obtained from the negative discriminant of the quadratic equation (7).

In Fig.2b, we show the Nyquist diagram for the kinetic case $0 < \eta < \eta_c$ where Im $\tilde{D}(\omega)$ is negative-definite for modes rotating in the ion diamagnetic direction. The diagram is *no* longer symmetric, and there is no condition on negative values of u_k for instability. There remains an instability condition for positive phase velocities given by

$$ku_k < \tilde{D}_A = 2k\gamma_0[1-C(\epsilon_n, \eta_i)] \qquad (16)$$

where C is given approximately by Eq.(14) as

$$C(\epsilon_n, \eta_i) = (2\epsilon_n)^{\frac{1}{2}} \frac{(1+2\eta_i)}{(1+\eta_i)^{3/2}}$$

valid for $C < 1$.

Finally, for $\eta > \eta_c$ the Nyquist diagram is as shown in Fig.2c, with the additional crossing of the Im $\tilde{D}(\omega)$ at $\omega = \omega_1$, where $\tilde{D}(\omega_1) = \tilde{D}_C$, which is easily shown to exceed $\tilde{D}_B$. This Nyquist diagram allows for the possibility of a new unstable mode at higher positive phase velocities such that

$$\tilde{D}_B < ku_k < \tilde{D}_C \qquad (17)$$

For the present model with $u_k = [1 - k^2(1+\eta_i) - 2\epsilon_n]/(1+k^2)$, this condition (17) is not satisfied, and thus there remains for $\eta > \eta_c$ only the one unstable mode given by condition (16), $ku_k < \tilde{D}_A(k, \epsilon_n, \eta_i)$. A change in u_k can, however, lead to condition (17) being satisfied. In particular, including the upward shift in the electron drift wave phase velocity due to its coupling with the ion acoustic wave allows u_k to satisfy condition (17).

Now, we consider the instability condition for finite ϵ_n and increasing η. For a fixed wavenumber k, as the temperature gradient increases, the phase velocity of the fluctuation decreases until instability occurs. For example, with the parameters $k = \sqrt{b\theta} = 0.3$ and $\epsilon_n = 0.1$ considered by Guzdar et al. [8] in their Fig.8, we obtain from the approximate kinetic instability condition

$$1 - k^2(1+\eta_i) - 2\epsilon_n < 2\gamma_0 - \frac{4\epsilon_n(1+2\eta_i)}{1+\eta_i} \qquad (18)$$

the threshold gradient of $\eta_t \cong 1$ compared with their value of $\eta_t \cong 2$. The fluid theory is already well into the unstable regime at $\eta_i = 1$ as shown in their Fig.9 or given by Eqs (7) and (8). Two factors contribute to the lower η_t value obtained from Eq.(18) relative to the value of Guzdar et al. One is that, for this example, k, q, and ϵ_n happen to be chosen such that $kq \sim \epsilon_n^{1/2}$. This is the transition regime between strongly ballooning and weakly ballooning wave functions. Secondly, in this example, the kinetic correction term is already one half the fluid term so that the asymptotic fluid expansion fails. Numerical evaluations show

that, for $\epsilon_n \gtrsim 0.1$, marginal stability must be computed with the full $E_1(z)$ response function. In this kinetic regime, we find that

$$\tilde{D}_A \simeq k(0.5+0.1\eta + \epsilon_n) \qquad (19)$$

is approximately valid for $\tilde{D}_A < \tilde{D}_B = k$ or $\eta \lesssim 5$. The instability condition obtained from $ku_k < \tilde{D}_A$ can now be written as

$$\eta(k^2+0.1) + k^2 + 3\epsilon_n > 0.5 \qquad (20)$$

which clearly shows the de-stabilizing effect of increasing either η, ϵ_n, or k^2. For the parameters $k^2 \cong \epsilon_n = 0.1$ and $\eta = 1$ condition (19) is marginally satisfied. The Nyquist diagram corresponding to this kinetic regime is identical in topology with that of Fig. 2b with the value of D_A given in Eq.(19). We observe that, in this regime, the second unstable domain of the Nyquist loop in Fig. 2c is removed.

We note that with the inclusion of electron-wave dissipation from trapped electrons, for example, the ω-term in the dispersion relation becomes $\omega(1-i\delta_k^e)$. Although the low-frequency part of the Nyquist diagram is unaffected, the high-frequency part is rotated by δ_k^e such that fluctuations with positive phase velocities of order unity are unstable when $\delta_k^e > 0$ with $\gamma_k \sim ku_k\delta_k^e$.

2.3. Large-wavenumber domain

Now we consider the higher-k modes which are stable according to fluid theory, diagram 2a and Eq.(8), but unstable in the kinetic theory, diagrams 2b and 2c. We rewrite the dispersion relation (6) as

$$\omega = ku_k - 2k^2\epsilon_n \int_0^\infty \frac{(1-\eta+\eta t)te^{-t}dt}{\omega+2k\epsilon_n t} \qquad (21)$$

In the region $|u_k| > 2\gamma_0$, we have

$$\omega = \tfrac{1}{2}ku_k + \left[(\tfrac{1}{2}ku_k)^2 - (k\gamma_0)^2\right]^{\frac{1}{2}} \lesssim ku_k$$

in the fluid domain. Iterating Eq.(18) with $\omega \cong ku_k$ yields

$$\omega_k + i\gamma_k = ku_k - 2kP\int_0^\infty \frac{(1-\eta+\eta t)te^{-t}dt}{u_k+2\epsilon_n t} + i\pi k\left(1-\eta-\frac{\eta u_k}{2\epsilon_n}\right)\left(\frac{-u_k}{2\epsilon_n}\right)\exp\left(\frac{u_k}{2\epsilon_n}\right) \qquad (22)$$

for $u_k < 0$. Not too far into the fluid regime, we have $u_k \sim -2\gamma_0$, and the resonant growth rate in expression (22) becomes

$$\gamma_k = \pi k\frac{\eta(1+\eta)}{2\epsilon_n}\exp\left[-\left(\frac{1+\eta}{2\epsilon_n}\right)^{\frac{1}{2}}\right] \qquad (23)$$

The Nyquist analysis shows instability for all positive k greater than the onset wavenumber given by Eq.(20); as is, however, evident from Figs 3, 4 and 5, there is an effective cut-off wavenumber k_c above which the growth rate is irrelevant. The cut-off wavenumber can be obtained by estimating the energy above which there is an insignificant number of resonant ions. For the Maxwell-Boltzmann distribution, we use Eq.(22) with the estimate that $\max(-u_k/2\epsilon_n) = 5$.

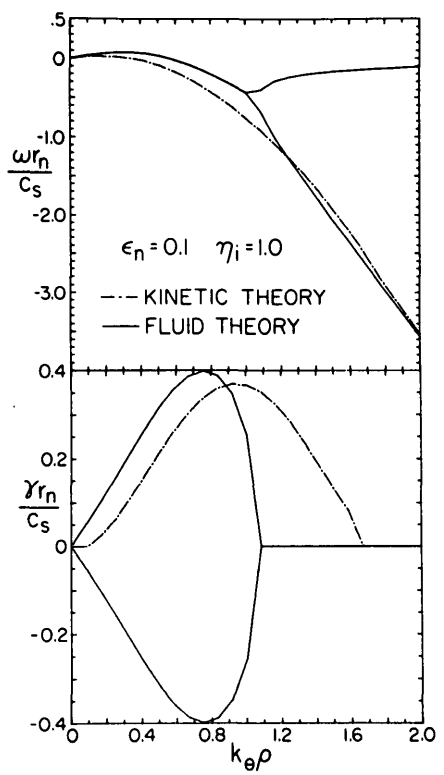

FIG. 3. Frequency and growth rate as functions of azimuthal wavenumber compared between the fluid theory and the kinetic theory for moderate aspect ratio.

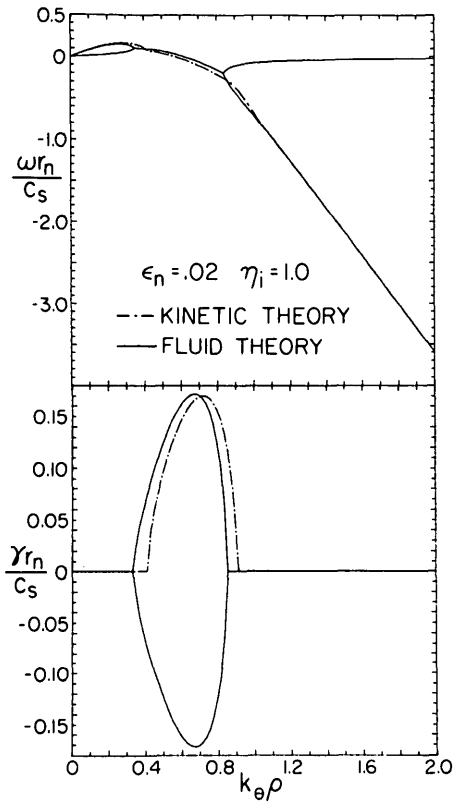

FIG.4. Same comparison as in Fig.3 for small aspect ratio where the fluid approximation is asymptotically convergent.

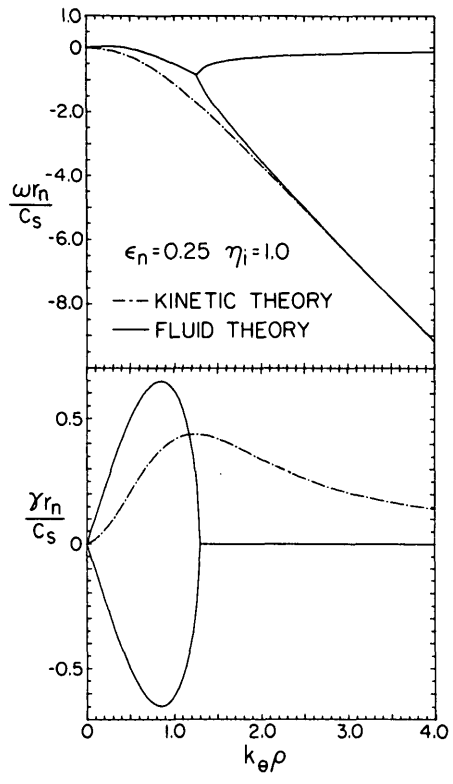

FIG.5. Same comparison given in Fig.3 for a large aspect ratio where the fluid approximation fails.

Solving this condition for the wavenumber gives

$$k_c = \left(\frac{1+12\epsilon_n}{1+\eta_i}\right)^{\frac{1}{2}} \tag{24}$$

for the critical wavenumber above which the growth rate is exponentially small.

For $\epsilon_n \gtrsim 0.1$ the critical wavenumber k_c given by Eq.(24) falls in a region where it is no longer justifiable to expand the Bessel function in Eq.(6). While the growth rate in this regime changes in magnitude, the topology of the Nyquist diagram and the sign of the growth rate remain the same. To show this, we note that with the Bessel function retained the imaginary part of $D(\omega)$ becomes

$$\mathrm{Im}D(\omega) = \pi k\left[1-\eta_i\left(\frac{\omega}{2\epsilon_n k} + 1\right)\right]$$

$$\times \left(\frac{\omega}{2\epsilon_n k}\right) J_o^2\left(k\sqrt{\frac{-\omega}{\epsilon_n k}}\right) \exp\left(\frac{\omega}{2\epsilon_n k}\right)$$

for $\omega < 0$. Clearly, the Bessel function does not change the sign of Im $D(\omega)$ for it enters as the square; rather it forces Im $D(\omega)$ to vanish at the roots of $J_0(x) = 0$. For moderate values of $k(k \lesssim 1.7)$, the zeros occur where the exponential falloff is already dominant and their effect is negligible. For higher values of k, this regime has been analysed with the Nyquist diagrams using the large-argument asymptotic expansion of the Bessel function while repeating the considerations given above with the small-argument expansion. Some non-resonant results for large k are given by Coppi and Pegoraro [2]. Here, we note that, in the non-resonant regime, the growth rate becomes $\gamma_k = (k\epsilon_n)^{1/2}(1+\frac{1}{2}\eta_i)^{1/2}/(2\sqrt{2\pi})^{1/2}$ valid for $1 \ll k \ll (1+\frac{1}{2}\eta_i)/8\sqrt{(2\pi)\epsilon_n}$, where the upper limit on k follows from the condition $\gamma_k > 2k\epsilon_n$.

The most important effect introduced by the Bessel function $J_0(k_\perp v_\perp/\Omega)$ is the change in the phase velocity u_k which enters the marginal stability criteria in Eqs (15) to (17). For $k \gtrsim 1$, the phase velocity of the drift wave is given by

$$u_k = \frac{\left\{I_o(k^2) + \eta_i k^2 [I_1(k^2) - I_o(k^2)]\right\} \exp(-k^2)}{2 - I_o(k^2)\exp(-k^2)} \tag{25}$$

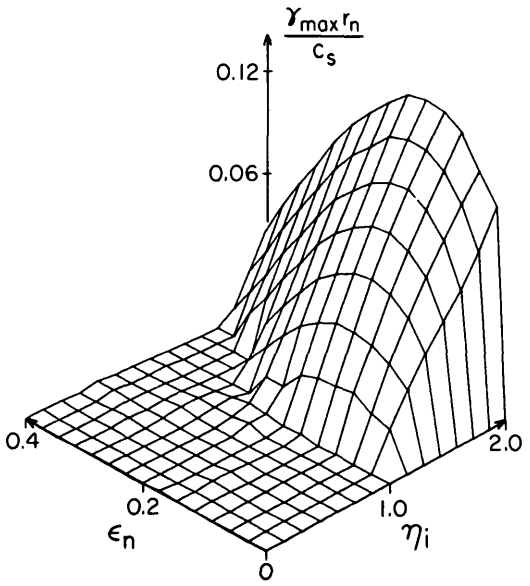

FIG. 6. The growth rate maximized over k for the grad-B model [Eq.(5)] showing the curve of marginal stability in the ϵ_n-η_i plane.

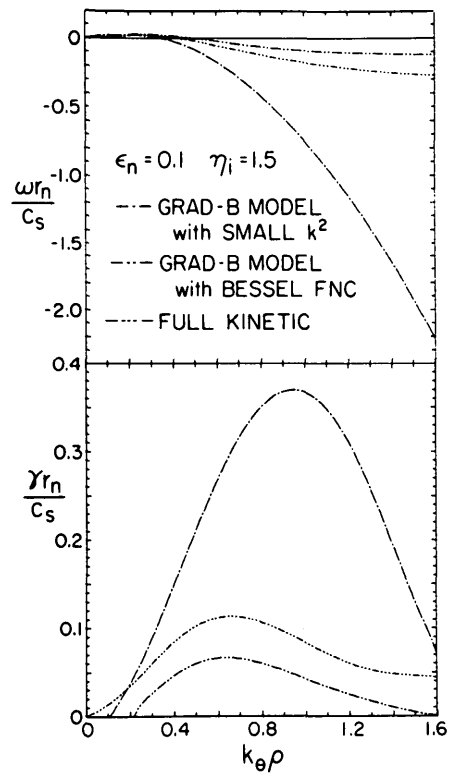

FIG. 7. The growth rate as a function of azimuthal wavenumber computed from the full kinetic dispersion function, [Eq.(4)], the grad-B model[Eq.(5)], and the grad-B model approximated for small k by the Bessel function expansion [Eq.(6)].

which has the small-k limit used in the fluid-theory analysis and the large k limit given by $u_k \cong (1-\frac{1}{2}\eta_i)/2\sqrt{2\pi k}$. The fact that for $\eta_i \lesssim 1$ the phase velocity given by Eq.(25) is appreciably larger than the fluid phase velocity in the region of the critical wavenumber $k \cong k_0 \cong (1+\eta_i)^{-1/2}$ prevents the instability conditions in Eqs (15) – (17) from being satisfied. This effect is summarized in Figs 6 and 7. Figure 6 shows the growth rate maximized over k as a function of ϵ_n and η_i and includes the curve of marginal stability in the $\gamma_m = 0$ plane. Figure 7 shows that retention of the full Bessel function for large k has an important effect on the value of the growth rate. Extrapolating to large values of k, the growth rate formula obtained from the small-argument expansion of the Bessel function is seen to overestimate the magnitude of the growth rate.

3. CONCLUSIONS

This work gives the change in the fluid-theory growth rate due to resonant drift-kinetic effects. The consideration is analogous to that in the work of Seyler and Freidberg [9] for the kinetic effects on the magnetohydrodynamic modes.

Since the region of fluid marginal stability is kinetically unstable, because of resonant particle-wave interactions, the unstable domain extends to higher wavenumbers and the maximum growth rate is shifted to higher k. As an example, we show in Fig.3 the kinetic-theory frequency and growth rate obtained from numerical solutions of Eq.(6) compared with the fluid-theory formulas. In Fig.4, we reduce the toroidicity parameter ϵ_n to a small value to indicate the asymptotic convergence with $\epsilon_n \to 0$ to fluid theory.

In summary, our analysis of the local kinetic dispersion relation for the ballooning ion pressure-gradient drift mode gives formulas for the marginal stability conditions in the hydrodynamic ($\epsilon_n < 0.1$) and kinetic ($\epsilon_n > 0.1$) regimes. In the former regime, the kinetic dispersion relation gave a Nyquist topology differing from that of the fluid dispersion relation as shown in Fig.2, although the kinetic criterion for marginal stability, Eq.(18), agrees with fluid results when computed to the next-higher order in $\epsilon_n^{1/2}$. For $\epsilon_n > 0.1$, the mode is fully kinetic, and the criterion for marginal stability is given by Eq.(20).

Figures 5 and 7 show the importance of the drift resonance and finite-gyroradius effects to the basic fluid prediction of the growth rate. Finally, we observe that, by comparing the present local results with the non-local ballooning-theory calculations of Ref.[1],

the relative importance of ballooning, drift-kinetic resonances at $\omega = \omega_D$ and the finite-gyroradius effects can be inferred. For typical toroidal regimes with $\xi < 2q$, we conclude that the finite-gyroradius effects and the grad-B resonances dominate the ballooning effects in determining the growth rate.

Appendix: THE GRAD-B MODEL

Here, we investigate the approximation made in reducing the two-dimensional velocity integral in Eq.(4) to the one-dimensional grad-B model in Eq.(5). The full dispersion function in Eq.(4) requires

$$I(\omega) = \left\langle\left\langle G_{\omega,k}(t,u) J_o^2(k\sqrt{2t}) \right.\right. \left. \times \left[\omega + k\left(1-\tfrac{3}{2}\eta_i\right) + k\eta_i\left(t+u^2\right)\right] \right\rangle_u \Big\rangle_t \qquad \text{(A1)}$$

where

$$\langle\ \rangle_u = \pi^{-\frac{1}{2}} \int_{-\infty}^{+\infty} du\ e^{-u^2}$$

and

$$\langle\ \rangle_t = \int_0^{+\infty} dt\ e^{-t}$$

and the particle-wave propagator is

$$G_{\omega,k}(t,u) = \frac{1}{\omega + k\varepsilon_n\left(t+2u^2\right)} \qquad \text{(A2)}$$

We define a response function analogous to the plasma dispersion function $Z(\phi)$ of infinite-uniform-plasma theory by

$$\left\langle\left\langle G_{\omega,k} \right\rangle_u \right\rangle_t = (1/k\varepsilon_n)\ W(\omega/k\varepsilon_n)$$

where

$$W(\phi) = \left\langle\left\langle \frac{1}{\phi + t + 2u^2} \right\rangle_u \right\rangle_t \qquad \text{(A3)}$$

which has the fluid limit

$$W(\phi) \simeq \frac{1}{\phi}\left(1 - \frac{2}{\phi}\right) \quad \text{for } |\phi| >> 1 \qquad \text{(A4)}$$

Recognizing that, on the average, $v_\parallel^2 \sim \frac{1}{2} v_\perp^2$, there are the two following one-dimensional models for $W(\phi)$:

$$\text{grad-B model:} \quad W_g(\phi) = \left\langle \frac{1}{\phi + 2t} \right\rangle_t \qquad \text{(A5)}$$

$$\text{curvature model:} \quad W_c(\phi) = \left\langle \frac{1}{\phi + 4u^2} \right\rangle_u \qquad \text{(A6)}$$

which both have the same hydrodynamic limit and fluid growth rate as the complete response function. In Fig.8, we compare the real and imaginary parts of these dimensionless dispersion functions.

We note the generally good agreement of the exact function $W(\phi)$ with the grad-B approximation $W_g(\phi)$ and the poorer agreement of the exact function with

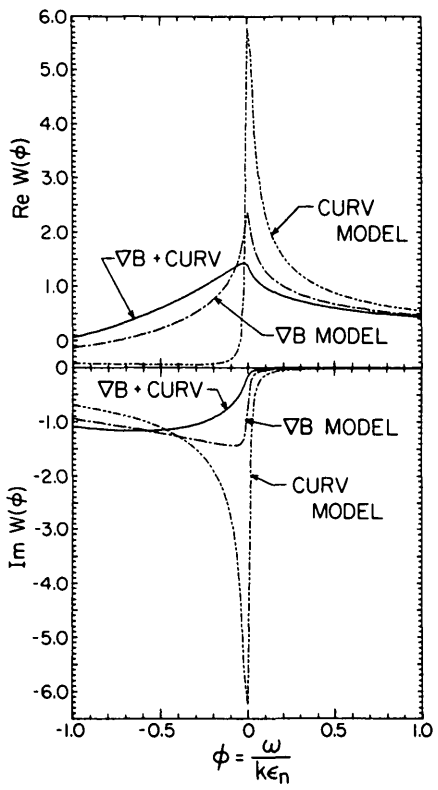

FIG.8. Comparison of dimensionless response functions $W(\phi)$, $W_g(\phi)$, and $W_c(\phi)$ as defined in the Appendix.

the curvature approximation $W_c(\phi)$. The most critical features of these functions in terms of marginal stability are the value of the imaginary part for $\phi<0$ and rate of fall-off of the real part for $\phi>0$. The disagreement between $W(\phi)$ and $W_g(\phi)$ near the origin $|\phi|<0.5$ only affects stability conditions for large values of ϵ_n. At $\epsilon_n=0.25$ the difference in the Nyquist diagrams obtained by replacing $W(\phi)$ by $W_g(\phi)$ becomes evident, with the most marked change occurring for the value of $\eta=\eta_c$, which is $\eta_c=1$ in the grad-B model. The overall effect is to increase the stability at this value of η for these large values of the toroidicity parameter.

When the mode is growing, the full dispersion function can be written exactly in terms of a one-dimensional integral. It is obtained by noting that for $\mathrm{Im}\,\phi=\mathrm{Im}(\omega/\epsilon_n k)>0$

$$\frac{1}{\phi+t+2u^2} = -i\int_0^\infty dy \quad \exp[iy(\phi+t+2u^2)] \tag{A7}$$

Equation (A1) then becomes

$$I(\omega) = -i\int_0^\infty dy \left\langle\left\langle \exp[iy(\phi+t+2u^2)]\; J_0^2(k\sqrt{2t}) \times [\omega+k(1-\tfrac{3}{2}\eta_i) + k\eta_i(t+u^2)] \right\rangle_u\right\rangle_t \tag{A8}$$

Both the u and the t integrations can now be performed so that $I(\omega)$ is expressed as an integral over y of a combination of modified Bessel functions I_0 and I, whose argument $\kappa=k^2/(1-iy)$ is a function of y:

$$I(\omega) = -i\int_0^\infty dy \exp[iy\phi] \times \left\{ \frac{e^{-\kappa}}{(1-iy)} \left[\frac{\alpha(1-2iy)+\frac{k\eta_i}{2}}{(1-2iy)^{3/2}} I_0(\kappa) + \frac{2k^3\eta_i}{(1-iy)\sqrt{1-2iy}} \times \left(I_0(\kappa) + \kappa\left(I_1(\kappa)-I_0(\kappa)\right)\right)\right]\right\} \tag{A9}$$

where

$$\alpha = \omega + k(1-\tfrac{3}{2}\eta_i)$$

While this form is exact, it is cumbersome analytically.

Formula (A7) is also useful in numerically evaluating the response function $W(\phi)$ of Eq.(A3). Substituting Eq.(A7) into Eq.(A3) yields

$$W(\phi) = -i\int_0^\infty dy \quad \frac{e^{iy\phi}}{(1-iy)(1-2iy)^{\frac{1}{2}}} \tag{A10}$$

the $(1-iy)^{-1}$ factor can be traced to the grad-B drift while the $(1-2iy)^{-1/2}$ factor is traceable to the curvature drift. Numerical evaluation of Eq.(A10) is facilitated by two separate transformations valid for $\phi>0$ and $\phi<0$. For $\phi>0$ we write

$$W(\phi) = \int_0^\infty \frac{e^{-\phi x}dx}{(1+x)(1+2x)^{\frac{1}{2}}} \tag{A11}$$

by transforming $y=ix$ and deforming the transformed contour to run from 0 to ∞. For $\phi<0$,

$$W(\phi) = -(1+i) \times \int_0^\infty \frac{\exp[(1+i)\phi x]\,dx}{[1-(1+i)x][1-2(1+i)x]^{\frac{1}{2}}} \tag{A12}$$

where we have used the transformation $y=\sqrt{2}\,x\exp(-i\pi/4)$ and shifted the contour to run from 0 to ∞. Both these transformations require that $|\mathrm{Re}\,\phi|>|\mathrm{Im}\,\phi|$. Both integrals (A11) and (A12) are rapidly convergent and convenient for numerical evaluations.

REFERENCES

[1] HORTON, W., CHOI, D.I., TANG, W.M., Phys. Fluids **24** 1077 (1981).

[2] COPPI, B., PEGORARO, F., Nucl. Fusion **17** (1977) 5.

[3] CHOI, D.I., HORTON, W., Phys. Fluids **23** (1980) 256.
[4] COPPI, B., ROSENBLUTH, M.N., SAGDEEV, R.Z., Phys. Fluids **10** (1967) 582.
[5] HORTON, W., ESTES, R.D., BISKAMP, D., Plasma Phys. **22** (1980) 663.
[6] TERRY, P., Theoretical Aspects of the Nonlinear Interaction of Drift-Type Instabilities in a Plasma, Ph.D. Dissertation, Austin, Texas (1981).
[7] ABRAMOWITZ, M., STEGUN, J.A., Handbook of Mathematical Functions, Dover, New York (1965) 228.
[8] GUZDAR, P.N., CHEN, L., TANG, W.M., RUTHERFORD, P.H., Ion-Temperature Gradient Instability in Toroidal Plasmas, Princeton Plasma Physics Report PPPL-1601 (1980).
[9] SEYLER, C.E., FREIDBERG, J.P., Phys. Fluids **23** (1980) 331.

(Manuscript received 2 March 1981
Final manuscript received 14 October 1981)